tion at all temperatures up to T_c in our tricrystal samples implies that d-wave symmetry predominates throughout. Our modeling gives best fit values of $\Phi = \Phi_0/2$ to within $\pm 10\%$ for all temperatures up to $T = 84$ K, ~ 6 K below T_c. Above this temperature, the Josephson penetration depths become very long, producing uncertainties in the fit parameters that diverge closer to T_c. To within the uncertainties assigned by our statistical analysis (as indicated by the error bars in Fig. 3B), there is no change in the total flux spontaneously generated at the tricrystal point at any temperature. Simple calculations indicate that, for example, an s-wave component to an $s + id$ superconducting order parameter would alter the flux quantization condition away from $\Phi_0/2$ by roughly the fractional portion that is s wave. We therefore conclude that the superconducting order parameter in YBCO is predominately d wave, with an imaginary component, if any, that is small from 0.5 K to T_c.

References and Notes

1. D. J. Scalapino, *Phys. Rep.* **250**, 329 (1995). An updated account of the phase-sensitive symmetry experiments appears in a review by C. C. Tsuei and J. R. Kirtley [*Physica C* **282–287**, 4 (1997)].
2. N. Bulut and D. J. Scalapino, *Phys. Rev. B* **54**, 14971 (1996).
3. S. M. Anlage et al., *ibid.* **50**, 523 (1994).
4. J. Ma et al., *Science* **267**, 862 (1995).
5. C. Kendziora, R. J. Kelley, M. Onellion, *Phys. Rev. Lett.* **77**, 727 (1996).
6. E. A. Pashitskii, V. I. Pentegov, A. V. Semenov, *Physica C* **282–287**, 1843 (1997).
7. N. E. Bickers, D. J. Scalapino, S. R. White, *Phys. Rev. Lett.* **62**, 961 (1989).
8. P. Monthoux, A. V. Balatsky, D. Pines, *Phys. Rev. B* **46**, 14803 (1992).
9. Conventional superconductors are invariant under time reversal. Certain possible unconventional pairing symmetries, such as $d_{x^2-y^2} + id_{xy}$, break this invariance.
10. S. Spielman et al., *Phys. Rev. Lett.* **68**, 3472 (1992).
11. J. R. Kirtley et al., *Nature* **373**, 225 (1995).
12. A. Mathai, Y. Gim, R. C. Black, A. Amar, F. C. Wellstood, *Phys. Rev. Lett.* **74**, 4523 (1995).
13. K. Suboki and M. Sigrist, *J. Phys. Soc. Jpn.* **65**, 3611 (1996).
14. M. Sigrist, D. B. Bailey, R. B. Laughlin, *Phys. Rev. Lett.* **74**, 3249 (1995).
15. M. Covington et al., *ibid.* **79**, 277 (1997).
16. G. Koren, E. Polturak, N. Levy, G. Deutscher, N. D. Zakharov, *Appl. Phys. Lett.* **73**, 3673 (1998).
17. K. Krishana, N. P. Ong, Q. Li, G. D. Gu, N. Koshizuka, *Science* **277**, 83 (1997).
18. D. A. Wollman, D. J. van Harlingen, W. C. Lee, D. M. Ginsberg, A. J. Leggett, *Phys. Rev. Lett.* **71**, 2134 (1993).
19. D. A. Brawner and H. R. Ott, *Phys. Rev. B* **50**, 6530 (1994).
20. C. C. Tsuei et al., *Phys. Rev. Lett.* **73**, 593 (1994).
21. J. H. Miller et al., *ibid.* **74**, 2347 (1995).
22. J. R. Kirtley et al., *Appl. Phys. Lett.* **74**, 4011 (1999).
23. These experiments use a Nb-AlO$_x$-Nb low-T_c SQUID with an integrated, well-shielded pickup loop. The SQUID is fabricated on a silicon substrate, which is connected through a highly thermally conducting copper cantilever and copper braid to the He$_4$ bath. The sample is scanned in relation to the SQUID with a lever mechanism. The sample and SQUID are in a vacuum space so that there is limited thermal conduction between them. The sample is heated with a thin-film resistor, and its temperature is measured with a silicon diode.
24. J. R. Kirtley et al., *Phys. Rev. Lett.* **76**, 1336 (1996).
25. B. J. Roth, N. G. Sepulveda, J. P. Wikswo, *J. Appl. Phys.* **65**, 361 (1988).
26. We thank G. Trafas for sample fabrication and M. B. Ketchen and M. Bhushan for the design and fabrication, respectively, of the SQUIDs used in this experiment. We also thank A. J. Turberfield for suggesting the concept behind our variable temperature scanning SQUID microscope.

Inhibition of Crystallite Growth in the Sol-Gel Synthesis of Nanocrystalline Metal Oxides

Nae-Lih Wu,[1]* Sze-Yen Wang,[1] I. A. Rusakova[2]

Crystal growth upon firing of hydrous transition metal oxide gels can be effectively inhibited by replacing the surface hydroxyl group before firing with another functional group that does not condense and that can produce small, secondary-phase particles that restrict advancing of grain boundaries at elevated temperatures. Accordingly, fully crystallized SnO$_2$, TiO$_2$, and ZrO$_2$ materials with mean crystallite sizes of ~ 20, 50, and 15 angstroms, respectively, were synthesized by replacing the hydroxyl group with methyl siloxyl before firing at 500°C. An ultrasensitive SnO$_2$-based chemical sensor resulting from the microstructural miniaturization was demonstrated.

Sol-gel synthesis is widely used for making transition metal oxide solids with fine-scaled microstructures. Pore and particle sizes no greater than a couple of nanometers can easily be achieved in the freshly derived gels. However, maintaining such microstructural dimensions when the fresh gels are subsequently crystallized at elevated temperatures is difficult. Freshly derived metal oxide gels have a hydrous solid skeleton that contains many hydroxyl groups and is either amorphous or paracrystalline. A postfiring step is therefore indispensable for dehydroxylation and for achieving a sufficient degree of crystallinity in order to give the desired combination of mechanical, catalytic, or optoelectronic properties for their applications. Upon firing of the gels, condensation among surface hydroxyl groups, nucleation of new oxide crystals, and growth of existing crystals occur concurrently over a fairly wide temperature range (*1, 2*). Accordingly, some crystals grow extensively before the gel is fully dehydroxylated and crystallized, which reduces surface area, enlarges pores, and increases the difficulty of removing intracrystal defects.

In the preparation of SnO$_2$ oxidation catalyst, for example, firing of the hydrous gel at 400°C for 1 hour removes <80% of the hydroxyl content but has already led to a fivefold increase in crystal size, from ~ 20 to 100 Å, and >50% loss in surface area and hence in catalytic activity (*2*). Firing hydrous ZrO$_2$ coating at

500°C is essential to giving sufficient thermomechanical strength for the high-temperature membrane reactor application, but pore sizes will more than triple, from 15 to 50 Å (see below). Destruction of the regular mesopore structures in the surfactant-templated metal oxide gels upon thermal treatment (*3*) is also likely caused by extensive crystal growth. Delayed crystal growth is thus the key to microstructural miniaturization of fully crystallized metal oxide materials prepared from the sol-gel and from other, similar wet processes.

Condensation of hydroxyl groups pulls together the constituent particles of the gel into a compact mass, and so the metal oxide crystals readily grow to a size much larger than that of the original particles. Accordingly, isolation of the hydrous particles upon firing may limit crystallization to taking place on a very local scale, and hence the original nanoscaled microstructure will be preserved. Second, crystal growth requires advancing of grain boundaries. Grain boundaries can be "pinned," and hence their motion restricted, by introducing tiny secondary-phase particles along grain boundaries. The challenge in the present case is to homogeneously introduce such "pinning" particles between crystals that are already nanoscaled. The surface hydroxyl groups appear to be perfect anchoring sites for the precursor species that would produce the particles. Therefore, an ideal approach that can simultaneously achieve both functions described above would be to replace the surface hydroxyl group with another functional group that does not condense as OH does and that could eventually form the "pins" at grain boundaries.
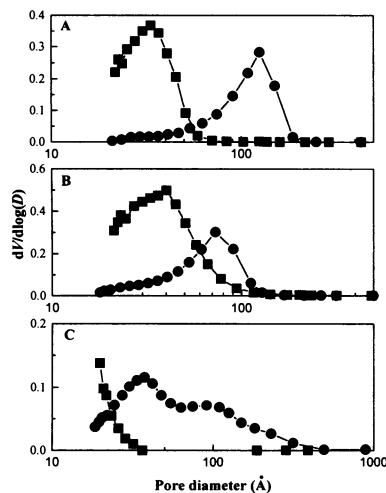
We tested this idea with particles of SnO$_2$, TiO$_2$, and ZrO$_2$, which are semiconducting ox-

^{1}Department of Chemical Engineering, National Taiwan University, Taipei, Taiwan 106, Republic of China. ^{2}Texas Center for Superconductivity at the University of Houston, Houston, TX 77204–5932, USA.

*To whom correspondence should be addressed. E-mail: nlw001@coms.ntu.edu.tw

**Fig. 1.** The Barrett-Joyner-Halenda pore size distributions determined by N_2 adsorption. (**A**) SnO_2, (**B**) TiO_2, and (**C**) ZrO_2 for (●) gels that were not treated with HMDS before firing and (■) gels that were first treated with HMDS. For the y axis, $dV/d\log(D)$, V represents pore volume and D pore diameter.

ides widely used in catalysts, sensors, membranes, transparent optical devices, and electrochemical capacitor electrodes. In all of these applications, small crystal size, high surface area, small pores, and a high degree of crystallinity are often preferred (4–7). Hexamethyldisilazane (8) {HMDS; $[Si(CH_3)_3]_2NH$} was selected as the OH-scavenging reagent because (i) it can replace the hydroxyl group in silica gel to form noncondensing methyl siloxyl surface group (9), and (ii) when decomposed in air above 350°C, it is expected to give SiO_2 particles, which could serve as the "pinning" particles.

The oxide gels were prepared by the spontaneous solution-sol-gel method (10), in

Table 1. Summary of the microstructural properties of the oxide xerogels. The specific surface area and mean pore size of the gels are determined by N_2 adsorption and calculated according to Brunauer-Emmett-Teller and Barrett-Joyner-Halenda formulations, respectively. The mean crystal sizes are calculated with Sherrer's equation based on the full width at half-maximum intensity in x-ray diffraction reflections ({110} for SnO_2, {101} for TiO_2, and {101} for ZrO_2). Full crystallinity and the quoted crystal sizes were confirmed by TEM micrographs and large-area diffraction patterns.

| Oxide	HMDS-treated	Specific surface area (m^2/g)	Mean pore size (Å)	Mean crystal size (Å)
SnO_2	No	40	150	200
SnO_2	Yes	133	32	20
TiO_2	No	56	59	150
TiO_2	Yes	223	36	50
ZrO_2	No	56	49	190
ZrO_2	Yes	139	25	15
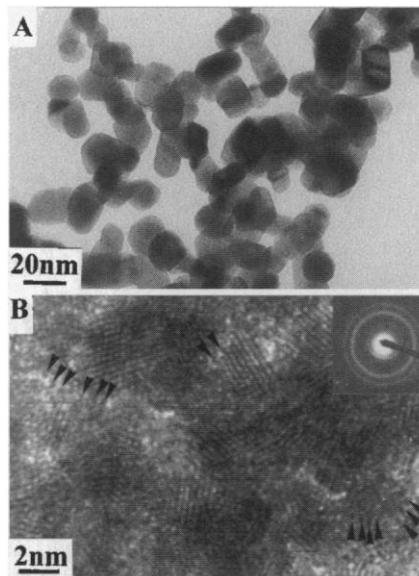
Fig. 2. Transmission electron micrographs of (**A**) U-SnO_2 and (**B**) H-SnO_2 gels fired at 500°C for 1 hour in air. The inset in (**B**) shows the large-area electron diffraction pattern, and the arrows indicate possible "pinning" particles.

which aqua-alcoholic solutions containing metal salts, including $SnCl_4\cdot5H_2O$, $TiCl_4$, and $ZrOCl_2\cdot8H_2O$, were aged at room temperature. Condensation took place spontaneously to produce gelatinous precipitate. The precipitate was then repeatedly washed with deionized water and finally either dried at 30°C under 75% humidity in air (xerogels) or subjected to CO_2 supercritical drying (aerogels). The HMDS treatment was carried out by placing the dried gels in a closed container, into which 5 ml of HMDS per gram of gel was injected. The entire container was heated at 150°C for at least 1 hour, during which time HMDS was expected to vaporize and react with the hydroxyl surface groups to form methyl siloxyl ones:

$$2 -OH + [Si(CH_3)_3]_2NH$$
$$\rightarrow 2 -OSi(CH_3)_3 + NH_3 \qquad (1)$$
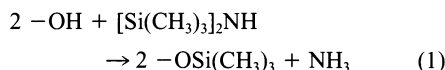
For firing, the gels, either with or without first being treated with HMDS, were heated at selected temperatures ranging from 200° to 500°C, for 1 hour. For simplicity, the prefix H will be used to denote samples that were treated with HMDS before firing, and U for those samples that were not treated with HMDS.

For SnO_2 gel, treatment with HMDS (reaction 1) significantly reduced the −OH absorption intensities (at 985, 1160, and 1442 nm) (2) and led to the appearance of the Sn-O-Si (980 cm^{-1}) (11) and Si-CH_3 (1250 cm^{-1}) (11) absorptions in the near-infrared (IR) and IR spectra, respectively. The IR spectra revealed that decomposition of the methyl siloxyl group began at 200° to 300°C and was complete below 500°C after 1 hour in air.
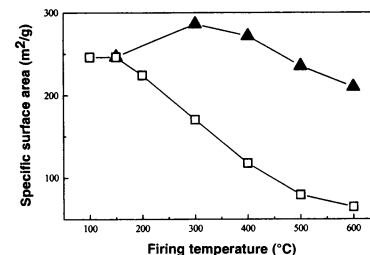

Fig. 3. The change in specific surface area of the CO_2-dried SnO_2 U-aerogel (□) and H-aerogel (▲) versus the gel-firing temperature.

Table 1 summarizes the microstructural properties of the xerogels, and Fig. 1 shows their pore size distributions. The fresh SnO_2 xerogel contains some crystallites ∼10 to 20 Å in diameter embedded in an amorphous matrix (2). After firing at 500°C for 1 hour, the mean crystal size (MCS) of U-gel increased to ∼200 Å (Fig. 2A), which is about 10 times that of the H-gel (Fig. 2B). Under the transmission electron microscope (TEM), we detected scattered small particles, 2 to 3 Å in diameter (arrows in Fig. 2B), between SnO_2 crystallites. Energy dispersive x-ray analysis using a converged beam on these particles gave silicon signals. They might be the "pinning" particles that result from the decomposition of the methyl siloxyl surface groups.

The CO_2-dried H-SnO_2 aerogels show an unusual temperature dependence on the specific surface area (SSA). Rather than dropping steadily with increasing firing temperature (as was seen with the U-aerogel), the SSA increased significantly when the H-aerogel was fired at 300°C (Fig. 3). This increase may result from the breakup of large agglomerates into small crystallites, exposing more surfaces. For U-gels, condensation among the hydroxyl groups occurs at lower temperatures than crystallization and only makes the agglomerates denser and less surface exposed. Hence, the surface-increase phenomenon does not occur upon direct firing of the hydrous gels. The H-aerogel retains an SSA of 210 m^2/g after firing at 600°C for 1 hour, whereas the U-aerogel has an SSA of only ∼70 m^2/g.

The quality of the SnO_2 crystallites can be evaluated on the basis of their ultraviolet (UV)-absorption edge profiles. SnO_2 cassiterite crystal has a theoretical absorption edge at ∼3350 Å, which can be observed experimentally for micrometer-sized SnO_2 crystals prepared by oxidation of tin at 1000°C (Fig. 4, curve 1). We have previously shown (2) a strong correlation between the UV absorption profile and the presence of defect structures. A confinement effect as a result of small crystallite size, which would cause a higher (blue-shifted) UV absorption edge, was not observed. Rather, structural defects formed during crystallization of the gel tend to introduce localized states within the gap near band edges
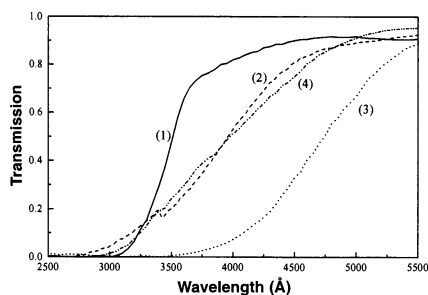
Fig. 4. The UV spectra of different SnO_2 materials. (1) Micrometer-sized crystals obtained from oxidation of tin at 1000°C; (2) H-gel fired at 500°C for 1 hour; (3) U-gel fired at 500°C for 1 hour; and (4) U-gel fired at 800°C for 1 hour.

Fig. 5. The response curves of CO sensors made of Pd-impregnated U-SnO_2 (dashed line) and H-SnO_2 (solid line) films at 20°C.

and result in a lower (red-shifted) absorption edge. Furthermore, after firing above 400°C, the red-shift decreases as defect density decreases. Although the H-grains fired at 500°C (MCS of ~20 Å) are 10 times smaller, they actually have a higher absorption edge energy (curve 2), that is, they have fewer defects than the U-grains (curve 3). Additional firing of the U-gel at 800°C for 1 hour gave the same UV absorption profile (curve 4) as that of the H-gel fired at 500°C, but its MCS increased to ~450 Å and its SSA dropped to 10 m²/g.

Firing of the H-TiO_2 gels at 500°C produces anatase crystallites with an MCS of 50 Å, as compared with 150 Å for the U-gel (Table 1). Under the same conditions, ZrO_2 gel crystallizes into the metastable tetragonal, rather than monolithic, crystallites with an MCS of 15 Å. For both oxides, the H-gels have a much greater SSA (Table 1) and smaller pore sizes (Fig. 1) than their U-gel counterparts.

Maintaining smaller crystal sizes can improve device performance. For example, in the following chemical-sensor application, Pd-containing SnO_2 films were prepared by first spin-coating the hydrous SnO_2 precipitate containing 1 mole percent Pd^{2+} onto silica substrates. The films, either treated or untreated with HMDS, were fired at 350°C for 1 hour. The fired films were subsequently exposed to atmospheres repeatedly switched between air and CO (500 ppm)–air mixture, and the resistances, R_{Air} and R_{CO}, respectively, were monitored with the four-point method. For polycrystalline conductors, grain boundaries contribute most of the resistance, especially when the intragrain defect density is low. The surface resistivity of an oxide crystal depends on the electron concentration near the surface, which in turn is affected by the nature of the chemisorbed species. Theoretically, the smaller the crystal size, the greater the sensitivity of overall resistance to the surrounding atmosphere.

The U-film showed a sensitivity (R_{Air}/R_{CO}) of 1.8 at 20°C, whereas the H-film gave an R_{Air}/R_{CO} ratio of ~90, a 50-fold increase (Fig. 5). The H-film is, in fact, an extremely
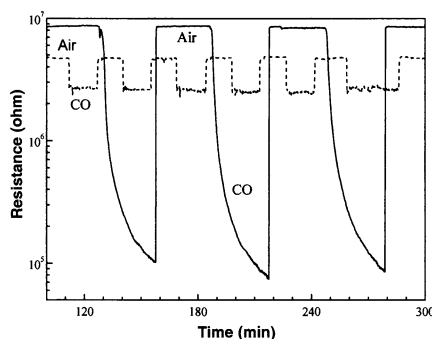
sensitive SnO_2-based CO sensor at room temperature, as typically the sensitivity of such films is no greater than 5.0 (*12*).

References and Notes
1. C. E. Brinker and G. W. Scherer, *Sol-Gel Sci.* (Academic Press, San Diego, CA, 1990), pp. 515–738.
2. N. L. Wu, L. F. Wu, I. A. Rusakova, A. Hamed, A. P. Litvinchuk, *J. Am. Ceram. Soc.* **82**, 67 (1999).
3. D. M. Antonelli and J. Y. Ying, *Angew. Chem. Int. Ed.*

Engl. **34**, 2014 (1995); L. Qi, J. Ma, H. Cheng, Z. Zhao, *Langmuir* **14**, 2579 (1998).
4. W. M. H. Sachtler and Y. Y. Huang, U.S. Patent 5,786,294.
5. K. Takahata, in *Chemical Sensor Technology*, T. Seiyama, Ed. (Elsevier, Amsterdam, 1988), vols. 1 and 2.
6. A. J. Burggraaf and K. Keizer, in *Inorganic Membranes: Synthesis, Characterization and Applications*, R. R. Bhave, Ed. (Van Nostrand Reinhold, New York, 1991), chap. 2.
7. Japanese Patent 2-1104.
8. Experiments with trimethylchlorosilane (TMCS) have also been performed and have given similar results. However, HMDS is less corrosive and much easier to handle than TMCS.
9. C. M. Jin, J. D. Luttmer, D. M. Smith, T. A. Ramos, *MRS Bull.* **22** (no. 10), 39 (1997).
10. N. L. Wu, L. F. Wu, Y. C. Yang, S. J. Huang, *J. Mater. Res.* **11**, 813 (1996).
11. *Infrared Structural Correlation Tables and Data Cards*, R. G. J. Miller and H. Willis, Eds. (Heyden, London, 1969), tables 9-A2a and 9-x3.
12. P. Bonzi *et al.*, *J. Mater. Res.* **9**, 1250 (1994); A. Nakajima, *J. Mater. Sci. Lett.* **12**, 1778 (1993); G. S. V. Coles, K. J. Gallagher, J. Watson, U. K. Patent GB 2177215.
13. Supported by the National Science Council of the Republic of China under contract NSC86-2113-M-002-006. TEM work was supported by the State of Texas through funding for the Texas Center for Superconductivity at the University of Houston.

16 April 1999; accepted 12 July 1999

Asteroidal Water Within Fluid Inclusion–Bearing Halite in an H5 Chondrite, Monahans (1998)

Michael E. Zolensky,[1]* Robert J. Bodnar,[2] Everett K. Gibson Jr.,[1] Laurence E. Nyquist,[1] Young Reese,[3] Chi-Yu Shih,[3] Henry Wiesmann[3]

Crystals of halite and sylvite within the Monahans (1998) H5 chondrite contain aqueous fluid inclusions. The fluids are dominantly sodium chloride–potassium chloride brines, but they also contain divalent cations such as iron, magnesium, or calcium. Two possible origins for the brines are indigenous fluids flowing within the asteroid and exogenous fluids delivered into the asteroid surface from a salt-containing icy object.

Over the past three decades, we have become increasingly aware of the fundamental importance of water and aqueous alteration on primitive solar system bodies. Some carbonaceous and ordinary chondrites, long touted as primordial material relatively unchanged since formation, have been altered by interactions with liquid water within the first 10 million years after formation of their parent asteroids (*1*). Nevertheless, we do not know the location and timing of the aqueous alteration or the nature of the aqueous fluid itself.

Workers have attempted to model and understand this aqueous process through analysis of hydrated minerals present in the meteorites and through computer simulations of the alteration process (*2*). A major impediment to our understanding of aqueous alteration has been the absence of actual samples of aqueous fluids in meteorites. Here, we report the discovery and characterization of aqueous fluid inclusions in an ordinary chondrite.

The Monahans (1998) (hereafter Monahans) ordinary chondrite fell on 22 March 1998 in Monahans, Texas. The fall was witnessed by seven boys, and the first of two stones was recovered immediately. This first stone was carried to the Johnson Space Center and broken open in a filtered-air, clean-room facility <48 hours after the fall, effectively eliminating the opportunity for aqueous or other contamination

[1]Mail Code SN2, NASA Johnson Space Center, Houston, TX 77058, USA. [2]Department of Geological Sciences, Virginia Tech, Blacksburg, VA 24061, USA. [3]Lockheed Martin Space Operations Company, Houston, TX 77058, USA.

*To whom correspondence should be addressed.